Supporting Information

Wilking et al. 10.1073/pnas.1216376110

SI Text

Evaporation Rate Estimate Using the Diffusion Limited Evaporation Approach. In the framework where evaporation is determined by the diffusion of water vapor in air, an estimate of the evaporation rate can be obtained that agrees well with the value measured for the biofilm. Consider a droplet of water sitting on the surface and having the same footprint as the biofilm. We assume that water vapor is saturated at the surface of the droplet with vapor concentration c_s and that far away from the droplet the vapor concentration c_∞ is set by the ambient humidity. The concentration of the water vapor above the droplet is given by the stationary solution of the diffusion equation. In this case the answer of the evaporation rate of the droplet is equivalent to calculation of the capacitance of a conducting body with the same shape as the droplet (1). It scales as a square root of the surface area of the droplet and contains a geometrical factor that weakly depends on the shape of the surface (2). For the hemispherical droplet of the radius R, the geometrical factor is 1 and the rate is given by

$$\frac{dm}{dt} = -2\pi D_v R\left(c_s - c_\infty\right),$$

where D_v is the diffusion constant of water vapor in air. We use the following values for parameters: $c_s = 20$ g/m^3 and $c_\infty = 4$ g/m^3 for relative humidity of 20% and room temperature 23 °C; radius of the footprint of the biofilm $R = 8.5{\cdot}10^{-2}$ m; the diffusion constant of water vapor in air is $D_v = 2.6{\cdot}10^{-5}$ m^2/s. That results in the estimate for the evaporation rate: 22.6 μg/s. Evaporation rate from a disk of the same radius as the footprint of the biofilm can be calculated by taking into account that the area of the disk is four times less than that of the sphere with the same radius, and the geometric factor for the disk is equal to 0.9 (3), leading to the value of 10 μg/s. Note that biofilm has a geometry resembling a disk rather than a sphere, but it also has a very wrinkled structure that increases its surface area; in addition, it is not just water but a complex structure of bacteria and polymer matrix. It is therefore surprising how close the theoretical estimate and measured values are.

Calculation of Hydrodynamic Resistance Across the Agar. From a liquid flow velocity of $V_z \approx 0.1$ μm/s we calculate the pressure drop necessary to drive water through the agar, using Darcy's law, $\Delta P_{D,agar} = (\eta L V_z)/k$, where η is the viscosity of water, L is the thickness of the agar, and k is the permeability of the agar. For $\eta \approx 10^{-3}$ Pa·s, $L \approx 0.5$ mm, $V_z \approx 0.1$ μm/s, and $k \approx 600$ nm^2 measured for 2 wt % agarose gels (4) we arrive at the result $\Delta P_{D,agar} \approx 0.83$ kPa ≈ 1 kPa.

Calculation of the Pressure Required to Compress the Agar. A biofilm exposed to ambient air with RH ≈ 20% will undergo evaporation at a rate $V_z \approx 0.1$ μm/s. An agar dish exposed for ∼30 min, the typical length of our experiments, will therefore lose enough water to decrease in thickness by an amount, $\Delta L \approx 0.180$ mm. This corresponds to a total volume change of $\Delta V/V = \Delta L/L = 0.180$ mm/5 mm = 0.036. The pressure required to compress the agar through the removal of water, $\Delta P_{compress}$, is set by the bulk osmotic modulus, K, where $\Delta P_{compress} = K(\Delta V/V)$. From a literature value of $K \approx 5$ kPa for an agar gel of 5 wt %, which we estimate from the slope of the equilibrium pressure-concentration curve in reference (5), and $\Delta V/V \approx 0.036$, we calculate $\Delta P_{compress} \approx 180$ Pa. Our agar gels are 1.5 wt %, so we expect $\Delta P_{compress}$ to be at least a factor of 2 less than this value we calculate.

Measurement of Permeability of the Biofilm. To measure the hydraulic permeability of the biofilm, k, we grew multiple *B. subtilis* biofilms under standard conditions, on agar plates, removed the biofilms from the agar plates and combined them into a bulk mass. The combined biofilm mass was centrifuged to remove air bubbles and loaded into a membrane filter. The biofilm was confined on either end by a membrane filter (pore size of 5 μm) and the thickness L of the biofilm pellet was set by a spacer of thickness $L = 2.4$ mm. Once loaded, the filter apparatus was attached to a syringe containing a filtered, liquid solution of the MSgg media. The media was forced through the biofilm with a pressure $\Delta P = 2.47{\cdot}10^4$ Pa, which was applied by simply placing a weight on the plunger of the syringe. The pressure drop through the apparatus, in the absence of the biofilm pellet, was measured to be negligible. The permeability is calculated from Darcy's law, $k = Q\eta L/\Delta PA$. For $Q \approx 3.08{\cdot}10^{-11}$ m^3/s, $\eta = 10^{-3}$ Pa·s, $L = 2.4{\cdot}10^{-3}$ m, $\Delta P = 2.47{\cdot}10^4$ Pa, and $A = 3.8{\cdot}10^{-4}$ m^2, we calculate k to be $0.78{\cdot}10^{-17}$ m^2, or ≈ 8 nm^2. To compare this measured value of the permeability of the biofilm with a theoretical estimate, we consider the microstructure of the biofilm, which consists of densely packed bacteria, with the interstitial space filled with an extracellular matrix. We neglect the contribution of the extracellular matrix and the anisotropy of the bacteria and use the empirical formula of Rumpf and Gupte for the permeability of densely packed hard spheres, $k = \frac{(1-\varphi)^{5.5}}{5.6}d^2$. For a bacteria diameter of $d \approx 1$ μm and bacteria volume fraction $\varphi \approx 0.6$–0.8, determined from image analysis, we obtain $k \approx 25$ nm^2 and 1,156 nm^2. Although the lower limit of our estimated permeability is not far from our measured value, the discrepancy is not surprising, because we neglect the contribution of the extracellular matrix. Additional information regarding the properties of the matrix would allow us to more accurately estimate the permeability, and incorporation of the matrix into our estimate would likely reduce this discrepancy.

Calculation of Hydrodynamic Resistance Across the Biofilm. From a liquid flow velocity of $V_z \approx 0.1$ μm/s we calculate the pressure drop necessary to drive water through the biofilm, using Darcy's law, $\Delta P_{D,biofilm} = (\eta L V_z)/k$, where η is the viscosity of water, L is the thickness of the agar, and k is the permeability of the agar. For $\eta \approx 10^{-3}$ Pa·s, $L \approx 100$–200 μm, $V_z \approx 0.1$ μm/s, and $k \approx 8$ nm^2 we arrive at the result, 1.2 kPa $\leq \Delta P_{D,biofilm} \leq 2.4$.

Calculation of Pressure Drop Along a Biofilm Channel. To estimate the pressure difference along the channel that is necessary to drive the liquid flow at the velocities that we observe, we assume Poiseuille flow and use $\Delta P_{xy} \approx 8\eta L V_{xy}/a^2$, where η is the viscosity of water, L is the length of a channel, V_{xy} is the liquid velocity in the channel, and a is the radius of the channel. For $\eta = 10^{-3}$ Pa·s, $L = 1$ cm, $V_{xy} = 10$ μm/s and $a = 50$ μm, we calculate $\Delta P_{xy} \approx 0.3$ Pa.

1. Deegan RD, et al. (2000) Contact line deposits in an evaporating drop. *Phys Rev E Stat Phys Plasmas Fluids Relat Interdiscip Topics* 62(1 Pt B):756–765.

2. Picknett RG, Bexon R (1977) The evaporation of sessile or pendant drops in still air. *J Colloid Interface Sci* 61(2):336–350.

3. Chow YL, Yovanovich MM (1982) The shape factor of the capacitance of a conductor. *J Appl Phys* 53(12):8470–8475.
4. Johnson EM, Deen WM (1996) Hydraulic permeability of agarose gels. *AIChE Journal* 42(5):1220–1224.
5. Lips A, Hart PM, Clark AH (1988) Compressive de-swelling of biopolymer gels. *Food Hydrocolloids* 2(2):141–150.

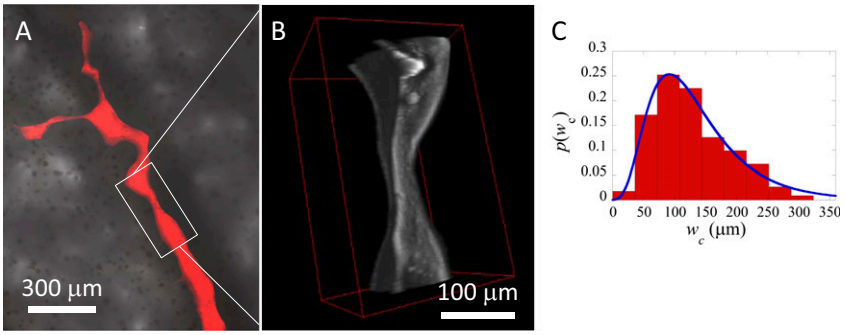

Fig. S1. To demonstrate the variability in the shape of a single channel section, we generate casts of the channels by introducing the resin directly into the center of a wrinkle (*A*) and plot the 3D reconstruction of the channel cast (*B*). To characterize the size of the channels in the network, we measure the maximum channel width, w_c, at 110 different, randomly selected points in the network of a biofilm (Fig. S5 *Left*) and plot the resulting probability distribution $p(w_c)$ in (*C*). The data are fit well with a log-normal distribution (blue line), which provides a mean and SD of $\overline{w_c} \approx 91\ \mu m \pm 65\ \mu m$.

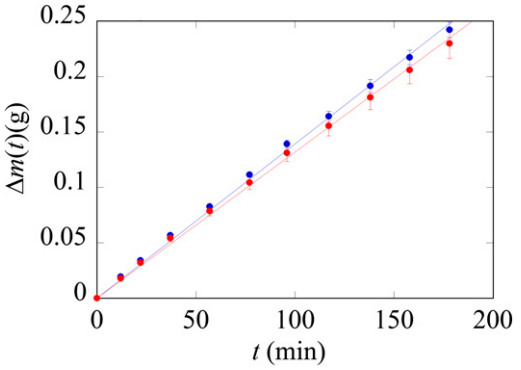

Fig. S2. Measured mass change due to evaporation from the surface of *B. subtilis* colonies (blue, 23.2 ± 0.5 μg/s) and agar slabs (red, 22.0 ± 1.2 μg/s) with diameters $d = 1.73 \pm 0.05$ cm exposed to a relative humidity of 19%.

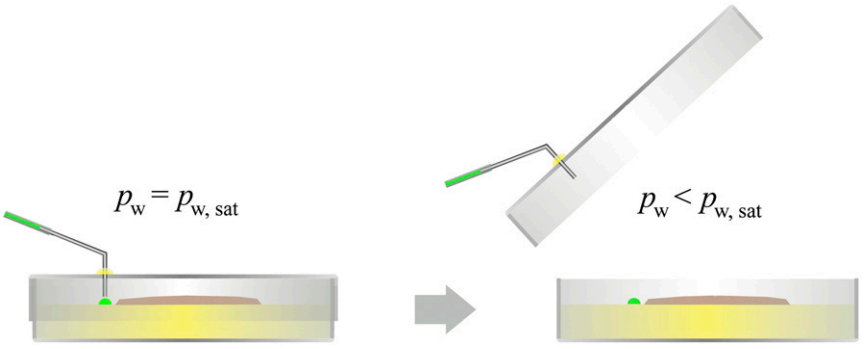

Fig. S3. Illustration of oil imbibition experiments. (*Left*) A biofilm sealed in a Petri dish for 2 h is blanketed in air with $p_w = p_{w,sat}$; an oil droplet is then placed in contact with the open end of a liquid-filled channel. No imbibition occurs. (*Right*) When the same biofilm is exposed to $p_w < p_{w,sat}$, imbibition occurs.

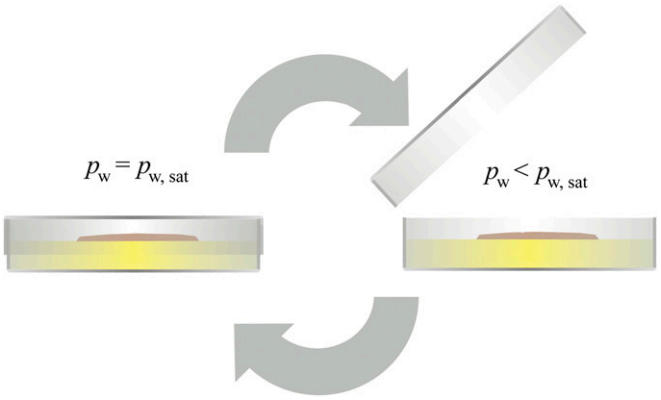

Fig. S4. Illustration of flow experiments. (*Left*) A biofilm sealed in a small Petri dish for 20 min is blanketed in air with $p_w = p_{w,sat}$, and no net flow velocity is observed in the channels. (*Right*) When the same biofilm is exposed to $p_w < p_{w,sat}$, directed flow in the channels is observed. For the experiment discussed in the manuscript (Fig. 3*D*), the Petri dish is covered and uncovered repeatedly.

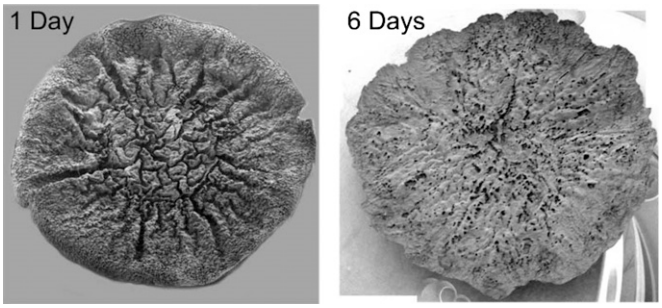

Fig. S5. Composite SEM images, formed by tiling high-resolution images, of the underside of two biofilms after 2 d of growth (*Left*) and 6 d of growth (*Right*). In the older biofilm, the biofilm has spread to cover the floor of the channels, and the network is not as open as in the 2-d biofilm. Most of the open holes in the 6-d-old biofilm are due to damage to the fragile sample during handling.

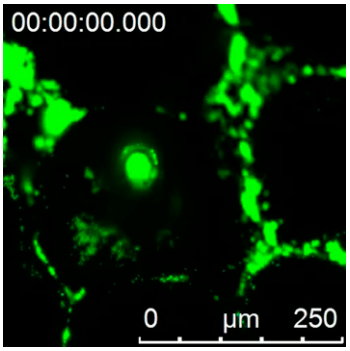

Movie S1. This move shows a tapered glass capillary (i.d. = 0.58 mm, o.d. = 1.0 mm, taper diameter ≈ 40 μm; World Precision Instruments), partially filled with an aqueous suspension of green fluorescent beads (d = 2 μm; Invitrogen), that is inserted into a network of wrinkles near the center of the biofilm. The liquid is spontaneously imbibed into the channel. Gravity is negligible here. There was intermittent clogging of the liquid flow in the end of the capillary, so the flow is not continuous (Quicktime; 761 kB).

Movie S1

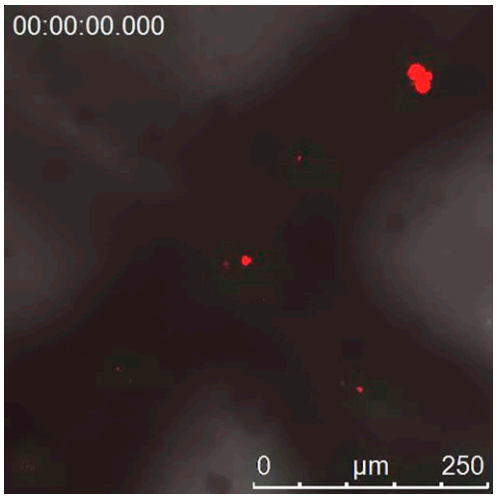

Movie S2. In this movie, the motion of fluorescent beads indicates that liquid flow rates on the order of 10 μm/s exist in the channels. A polydisperse suspension of fluorescent beads was prepared by emulsifying the Mercox II resin before cross-linking. A dilute solution of beads was imbibed into a channel, the capillary removed, and the system allowed to equilibrate for ~20 min before imaging the channels. During equilibration, the beads spread throughout the channel network, over distances >1 cm. (Quicktime; 234 kB).

Movie S2

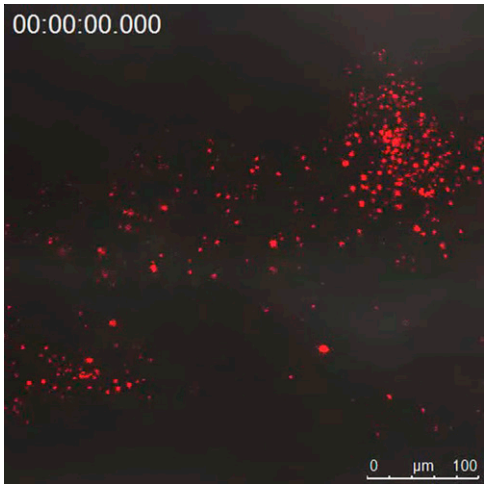

Movie S3. In this movie, the flow of water in a channel can be followed by tracking the motion of fluorescent beads suspended in the water. Initially, the biofilm is covered with a small Petri dish for several minutes, and no flow is observed. When the cover is removed ($t \approx 3$ min) flow rapidly commences and slows after the cover is replaced ($t \approx 4{:}45$ min). This effect is repeated; the removal and replacement of the cover is marked by changes in the background intensity of light. The experimental setup is illustrated in Fig. S4 (Quicktime; 16.1 MB).

Movie S3